Materials Advances

ROYAL SOCIETY OF CHEMISTRY

PAPER

View Article Online
View Journal

Cite this: DOI: 10.1039/d5ma01354b

Substituent-directed assembly of 1D and 2D silver aryl tellurolates with tunable emission

Komal Rani,[ab] Anietie W. Williams,[b] Tarun Kaushik,[ab] Daniel W. Paley,[c] Maggie C. Willson,[ab] Masha Aleksich,[ab] Patience A. Kotei,[ab] Mark R. Warren,[d] Adrian P. Mancuso,[de] Kerry Gilmore,[b] Aaron S. Brewster*[c] and J. Nathan Hohman*[ab]

Received 21st November 2025,
Accepted 8th April 2026

DOI: 10.1039/d5ma01354b

rsc.li/materials-advances

Metal–organic chalcogenolates (MOChas) are hybrid materials notable for excellent air and water stability and strong light-matter interactions. Tellurium-based MOChas have been limited to only a single example, tethrene (AgTePh). We modified a Grignard-based synthetic approach to prepare bis(4-methoxyphenyl) ditelluride and bis(3-methoxyphenyl) ditelluride, then prepared the corresponding MOChas. We used synchrotron serial crystallography at the Diamond Light Source, merging 90-degree sweeps from six selected microcrystals using "needle-in-a-haystack" approach to solve the crystal structure of AgTe-4M, revealing the tethrene-like 2-dimensional layered system. We also identified a bright red luminescent AgTe-3M derivative that is consistent with a 1-dimensional system. In parallel, we observed that elemental tellurium is a problematic contaminant that negatively impacts crystal morphology and yield when present during the synthesis. We demonstrate that inclusion of elemental tellurium is generally tolerated when <1% by weight.

Introduction

Strong light-matter interactions in metal–organic chalcogenolates (MOChas), particularly those produced using organic thiolates, selenolates, and tellurolates of coinage metals (Cu, Ag, Au) have recently drawn substantial interest.[1–11] These crystalline low-dimensional nanostructures exhibit chemical configurability, structural flexibility, and electronic tunability, enabling remarkable optoelectronic and mechanical properties.[12–21] We and others have been working to assemble a comprehensive MOCha library in pursuit of understanding how to integrate these compounds into potential applications as semiconductors, sensors and catalysts.[22–29] Tellurolate analogs remain largely underexplored in comparison to thiolates and selenolates. To fully understand the impact of chalcogen identity on properties such as dimensionality, the synthesis of tellurolates is essential. Tethrene, formally identified as silver benzenetellurolate (AgTePh),[6] remains the only reported crystal structure within the family of tellurium-based MOChas. A detailed comparison of tethrene with its sulfur and selenium-based counterparts suggests that tellurium-based MOChas exhibit unique electronic and photophysical properties, such as self-trapped excitons and broadband emission, offering potential for diverse optoelectronic applications including photodetectors, LEDs and light emitters.[8,30–35] The methodological developments for the synthesis of metal–organic tellurolates are essential for advancing systematic design and optimization of their optoelectronic properties.

MOChas have been prepared from a variety of silver sources, including elemental silver, silver nitrate, silver oxide, or by displacement of less nucleophilic MOChas.[36–39] We and others previously employed the redox reaction between diphenyl ditelluride and elemental silver[6,30] for the preparation of tethrene, and silver oxide has been used separately.[34] The synthetic procedure of using silver metal as a metal precursor follows a pathway where silver undergoes oxidation.[3,39] Expanding the synthetic library of tellurium-based MOChas has been slow due to the lack of commercial availability of tellurium-based ligands, so all new examples must be prepared by synthesizing tellurols/ditellurides. Thiols and selenols and their corresponding diselenides and disulfides are relatively straightforward to prepare synthetically; however, we have noted that it is considerably more laborious to prepare the corresponding tellurols.[33] Tellurium is the least electronegative and largest element of the three chalcogens. This makes nucleophilic insertion into Grignard or organolithium reagents (traditional synthesis pathways) particularly challenging. Also,

[a] Institute of Materials Science, University of Connecticut, CT, 06269, USA. E-mail: james.hohman@uconn.edu
[b] Department of Chemistry, University of Connecticut, CT, 06269, USA
[c] Molecular Biophysics and Integrated Bioimaging Division, Lawrence Berkeley National Laboratory, Berkeley, CA, 94720, USA. E-mail: asbrewster@lbl.gov
[d] Diamond Light Source, Harwell Science & Innovation Campus, Oxfordshire OX11 0DE, UK
[e] La Trobe University, Melbourne, VIC, 3086, Australia

tellurols are highly unstable and readily oxidize to ditellurides, making their direct use in MOChas synthesis is difficult.[40,41] Consequently, ditelluride ligands are preferred. However, the use of ditelluride ligands presents several unique technical challenges, particularly regarding their purity and stability: ditelluride ligands have been reported to decompose to tellurium metal and unidentified byproducts, potentially the monotellurides.[42,43]

Recently, we and others have examined structural transitions in MOChas by changing the aryl functional group position.[23] We hypothesized that the tethrene inorganic motif would be conserved.[22,23] Here, we prepared bis(4-methoxyphenyl) ditelluride, bis(3-methoxyphenyl) ditelluride, and their corresponding MOChas. We utilized a protocol for treating elemental tellurium with a Grignard reagent to prepare the ditellurides and used column chromatography to purify them for the preparation of the corresponding MOCha. We identified the crystal structure of the 2-dimensional silver 4-methoxybenzenetellurolate *via* synchrotron serial crystallography at the I19 beamline at the Diamond Light Source.[44] Emerging reports show a link between the functional group and its position on aryl ring and the dimensionality of silver thiolate and selenolate MOChas, with *para*-substitued derivatives forming 2D lamellar sheets and *meta*-substituted analogs yielding needle-like crystals comprised of 1D inorganic-polymers.[5,22,30,45] We show this case to be the same for the silver tellurides. We further identified a 1-dimensional motif for the 3-methoxy ligand, comparable to the corresponding 1-dimensional silver thiolates and report on the interesting optical phenomena between the 2D and 1D systems.

Results and discussions

We first prepared the MOChas AgTePh (tethrene), AgTe-4M (silver 4-methoxybenzenetellurolate) and AgTe-3M (silver 3-methoxybenzenetellurolate) shown in Fig. 2a. These molecules were synthesized to investigate the effect of methoxy functional group (–OCH_3) and the position of this functional group (*meta* & *para*) on phenyl ring in the organic layer of MOChas. The prime example of Te-based MOCha, AgTePh is a well-studied material and has been synthesized using approaches where silver metal or silver oxide can be used as a metal source.[6,30,34] We have used the earlier reported redox synthetic procedure[3] where, in a single step, Ag powder can be made to react with diphenylditelluride for oxidation–reduction. Ag(0) undergoes oxidation to form Ag(+1), and Te(0) undergoes reduction to form Te(−1) (Fig. 1). The oxidation character of chalcogens decreases down the group (S, Se, Te) with increasing size and, therefore, tellurium compounds are expected to be more challenging than S and Se. It was observed that the reaction needed a stable 80–85 °C for the formation of the expected product. The organic precursors bis(4-methoxyphenyl) ditelluride and bis(3-methoxyphenyl) ditelluride should be used instantly as MOCha reagents as they likely begin degrading immediately, forming the tellurium metal contaminant even at room temperature.[42,43] Chromatographic separation is an explicit necessity to remove any side products and, most importantly, tellurium metal. From the applied synthetic method, the recovered yield obtained for tethrene and AgTe-4M was 80–90% and 60–75% for AgTe-3M.

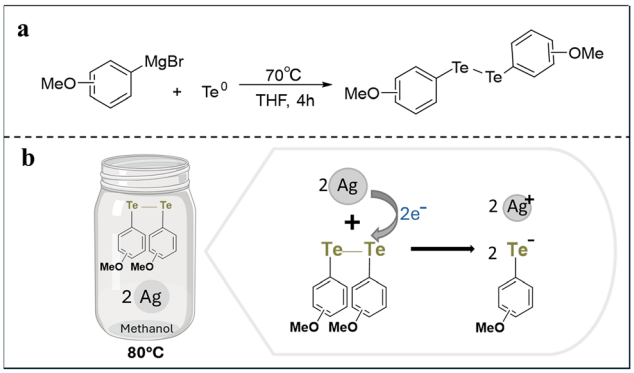

Fig. 1 Synthetic scheme shows conversion of Grignard reagent 3- or 4-methoxyphenylmagnesium bromide to bis(3- or 4-methoxyphenyl) ditelluride in the first step (a) and formation of MOChas by redox conversion in the second step (b).

Scanning electron microscopy (SEM) images shown in Fig. 2c and d reveal the difference in morphology and size of *meta*-substituted (AgTe-3M) and *para*-substituted (AgTe-4M) products. The crystal size of *para*-substituted crystals is typically in the range of 1–15 μm and 0.5–5 μm for *meta*-substituted product. The *para*-substituted aryl materials produce slanted-rectangular 2-D crystals with sharp edges, whereas the *meta*-functionalized product has a small, rod-like 1-D crystal habit, consistent with the corresponding methoxy substituted thiolates.[23] This observation suggests that the variation in chalcogen atom size has minimal influence on the crystal growth process, maintaining a consistent morphology. Instead, dimensionality is more strongly governed by the substituent position, with *para*-substituted MOChas favoring 2D structures, while the steric constraints in *ortho*- and *meta*-substituted derivatives predominantly lead to 1D formations.

The pXRD (powder X-ray diffraction) patterns shown in Fig. 2b follow the typical peak patterns of 2-D and 1-D crystals. Typically, 2-D layered materials have equally spaced intense peaks in the low angle region and 1-D has irregularly spaced peaks in the low angle region.[16,22,39,46–48] The pXRD and SEM results for both samples demonstrate a correlation between dimensionality, crystal shape, and peak spacing, which is consistent with observations in other MOCha crystal systems.[23,49,50]

Crystal structure determination

To determine the crystal structure of AgTe-4M, we used synchrotron serial crystallography at Diamond Light Source (DLS), whereas previous studies on this class of materials primarily employed smSFX.[6] At the I19 beamline at DLS, we efficiently scanned hundreds of crystals across multiple 400-well grids. For wells exhibiting diffraction, a wider rotation collection was performed, with the system demonstrating remarkable resilience to high X-ray doses. Serial methods typically merge hundreds or thousands of small datasets; however, in this case, the "needle-

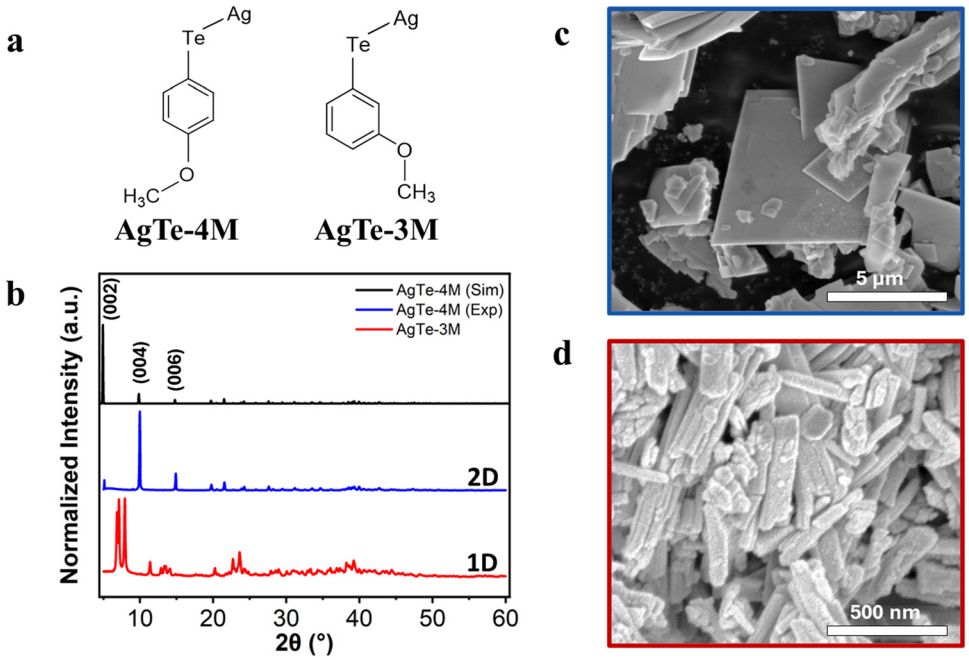

Fig. 2 (a) Formed MOCha products Silver 4-methoxybenzenetellurolate (AgTe-4M) and Silver 3-methyoxybenzenetellurolate (AgTe-3M) (b) Experimental powder pattern of AgTe-3M (Red), AgTe-4M (Blue) and simulated powder pattern of AgTe-4M (Black) (c) SEM showing morphology and size of 2-D AgTe-4M (d) Morphology and size of 1-D AgTe-3M.

in-a-haystack" approach allowed us to rapidly screen a large volume of material and selectively extract datasets with the best statistics. In this case, we identified six crystals with strong diffraction that could be merged to produce a complete dataset. Using this strategy, we successfully solved the AgTe-4M structure. This technique closely resembled conventional single-crystal determination, as data were collected using the rotation method once a high-quality candidate was identified.

Comparing AgTe-4M to its non-functionalized analogue, tethrene,[6] we observed that the functional group altered the crystal symmetry. The presence of heavy elements provided excellent scattering, even for such a small crystal. The system crystallizes in the orthorhombic space group *Cmce* (Fig. 3a, Table 1), whereas AgTePh, as reported, crystallizes in the monoclinic space group *C*2/*c*.

The arrangement of inorganic and organic layers depicts a lamellar structure. Fig. 3b shows the inorganic structural component: each silver is bonded to 4 tellurium atoms with Ag–Te bond lengths 2.826 Å and 2.923 Å. Silver-silver spacings in pure silver clusters range 2.5–2.8 Å.[51] Argentophilic interactions in silver-containing coordination compounds and in hybrid material systems extend up to 3.44 Å and are implicated as playing an important role in the emission properties.[51–54]

We now consider the internal organic interfaces. Methoxy groups adopt a generally tetrameric packing arrangement. In the solid state, the weak interactions between the dipolar functional groups stabilize tetrameric patterns in crystal structures as shown in Fig. 3c. The interactions between aliphatic hydrogen and oxygen atoms approach 2.48 Å. Such interactions are well-understood to have stabilizing effects on a variety of crystal systems.[55–58] In the AgTe-4M structure, intermolecular C–H···O interactions are observed between methoxy groups of adjacent organic layers, with a characteristic interaction distance of 2.533 Å. These are weak non-covalent interactions that contribute to the structural stability of the hybrid framework.

The thermogravimetric analysis (TGA) was performed on crystalline samples to determine the thermal stability, and results are shown in Fig. S1. The residue contains silver and tellurium after decomposition and loss of organic components. All three reported MOChas, AgTePh, AgTe-4M, AgTe-3M are thermally stable at high temperatures up to 220 °C and decomposition (5% weight loss) occurs at around 260 °C for AgTePh, 280 °C for AgTe-4M and 235 °C for AgTe-3M. The decomposition temperature for AgTe-4M is slightly higher than AgTePh, and this is attributed to the presence of additional non-covalent dipolar interactions in the supramolecular phase.

Studies have shown that low-dimensional materials have significant optoelectronic applications.[21,47] The optical properties of chalcogenide-based organic–inorganic hybrid frameworks can be optimized by varying composition and functionality.[33,59,60] Direct relationships between dimensionality and optical properties is shown in literature.[61,62] Fig. 4 shows the optical characterization of the three MOChas and reveals that all three visibly fall within a yellow-brown colour range. Visually, tethrene is a yellowish orange solid, AgTe-4M appears more brightly colored, and AgTe-3M is a darker brownish-yellow in visible light. Fig. 4a shows the MOChas in ambient light and 365 nm UV lamp to demonstrate that tethrene and AgTe-4M have similar yellow luminescence, whereas AgTe-3M shows bright red luminescence under UV lamp. Fig. 4b and c show fluorescence and absorption spectroscopy results that show similar broad emission peaks of tethrene and AgTe-4M in the

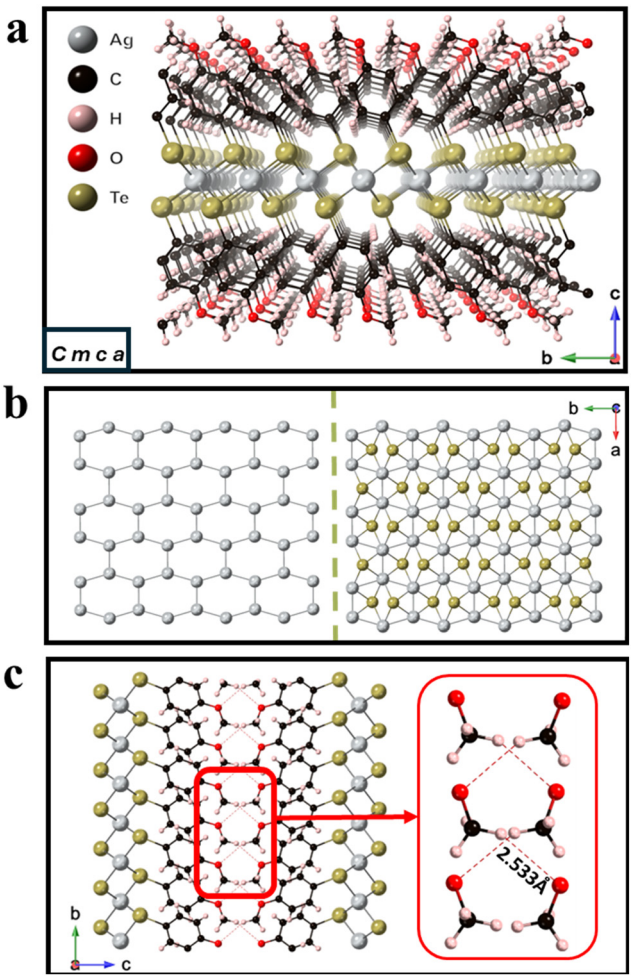

Fig. 3 (a) Orthorhombic Crystal System of Silver 4-methoxybenzenetellurolate with space group – *Cmce* (b) Hexagonal inorganic structure Ag–Ag and Ag–Te (c) Interlayer C–H–O interactions in methoxy groups.

broad orange region of ~520–690 nm wavelength and broad emission peak around 580 nm. Similar emissive properties in the two solids can be attributed to the close match in their structural parameters. AgTe-3M emits in the region ~600–850 nm with a peak emission around 700 nm. The shift in luminescence from broad yellow to red shows that optical properties of metal–organic telluride depend on the substituent's position.

Compared to silver coordinated thiolates and selenolates, the tellurium based MOChas exhibit distinct photoluminescence peroperties demonstrating chalcogen-dependent tuning of emission. While silver 4-methoxybenzenethiolate is non-luminescent, it's Te analog AgTe-4M emits in yellow-orange region and AgTe-3M displays a pronounced red shift corresponding to silver 3-methoxybenzenethiolate with peak emission at 589 nm. These observations highlight that substituent controlled structural variations and framework dimensionality govern the emissive properties of tellurium-based MOChas through extended Ag–Te–Ag network and stronger argentophilic interactions, consistent with trends reported for related chalcogenolate systems. AgTe-4M has two Ag–Ag interactions of 2.867 Å and 3.096 Å. The shorter interaction is closer to the distance in silver metal, implying strong coupling between the atoms. These are slightly elongated relative to tethrene, reported at 2.806 Å and 3.086 Å. Compared to silver 4-methoxybenzenethiolate, which is non-luminescent and has Ag–Ag distances of 2.973 Å and 3.669 Å similar to non-functionalized silver benzenethiolate, the AgTe-4M exhibit shorter distances.[23]

Table 1 Crystallographic data on parameters for AgTe-4M collected at diamond

Compound	AgTe-4M
Formula	$AgTeC_7H_7O$
MW	342.60
Space group	*Cmce*
a (Å)	7.4688(3)
b (Å)	5.9438(2)
c (Å)	35.972(2)
α (°)	90
β (°)	90
γ (°)	90
V (Å^3)	1596.90(10)
Z	8
ρ_{calc} (g cm^{-3})	2.850
X-ray source	DLS
λ (Å)	0.4859
T (K)	150.15
d_{min} (Å)	0.8
μ (mm^{-1})	2.202
Data	857
Restraints	56
Parameters	73
R_{int} (%)	20.51
R_1(obs) (%)	5.49
R_1(all) (%)	10.22
S	0.897
Peak, hole (e$^-$ Å^{-3})	1.643, −1.037

Negative effect of Te presence during synthesis

We identified a deleterious effect of elemental tellurium when present in a reaction mixture. We utilized the Grignard reaction to synthesize diphenyl ditelluride for comparison with a commercial source. However, the resulting products were typically brown solids with irregular needle-like crystal habits in contrast to the pristine tabular crystals recovered using commercial diphenyl ditelluride. We identified traces of elemental tellurium in the synthetic precursor after filtration and in the final product during the purification process. We attributed the presence of the tellurium to the lower quality of the resultant MOCha. This is synthetically straightforward to resolve, as the precursor was purified using column chromatography before proceeding with the reaction, which yielded the desired result.

To assess the contamination threshold, a sequence of experiments was performed to deliberately introduce different proportions of elemental tellurium into the reaction. AgTePh formed without the addition of tellurium metal in the reaction system is labeled as 0%. While reaction mixtures containing 0.01 mg, 0.02 mg, and 0.05 mg of tellurium per mg of organic precursor are labeled as 1%, 2%, and 5% respectively. The recovered yield decreased from 85–90% to 20% with increase in

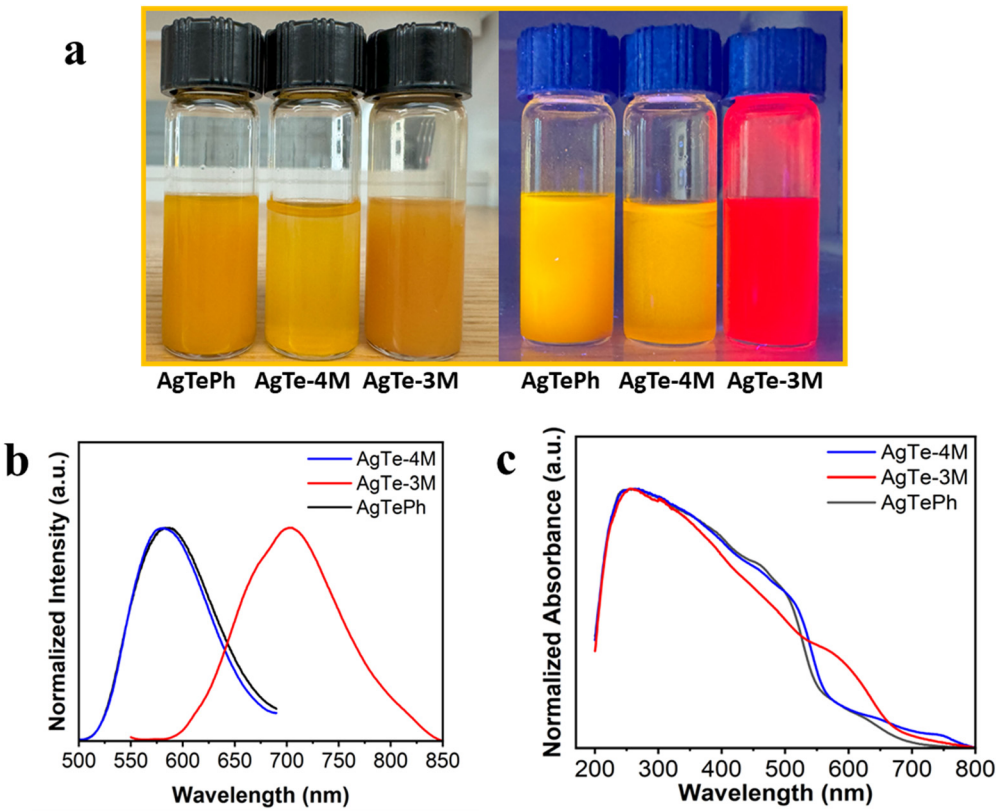

Fig. 4 (a) Images of suspended solution (1 mg ml^{-1} in methanol) of species AgTePh, AgTe-4M & AgTe-3M under ambient light and 365 nm UV lamp (b) Normalized emission spectra in the region 500–850 nm (c) Normalized absorption spectra in the region 200–800 nm.

elemental tellurium from 0 to 5%. Fig. 5a shows the SEM images of these samples revealing that increasing tellurium contamination correlates with smaller crystals and a rough appearance to the product crystal faces. Fig. 5b shows the negative correlation of increasing tellurium impurity on the optical emission of the product, consistent with lower yield and

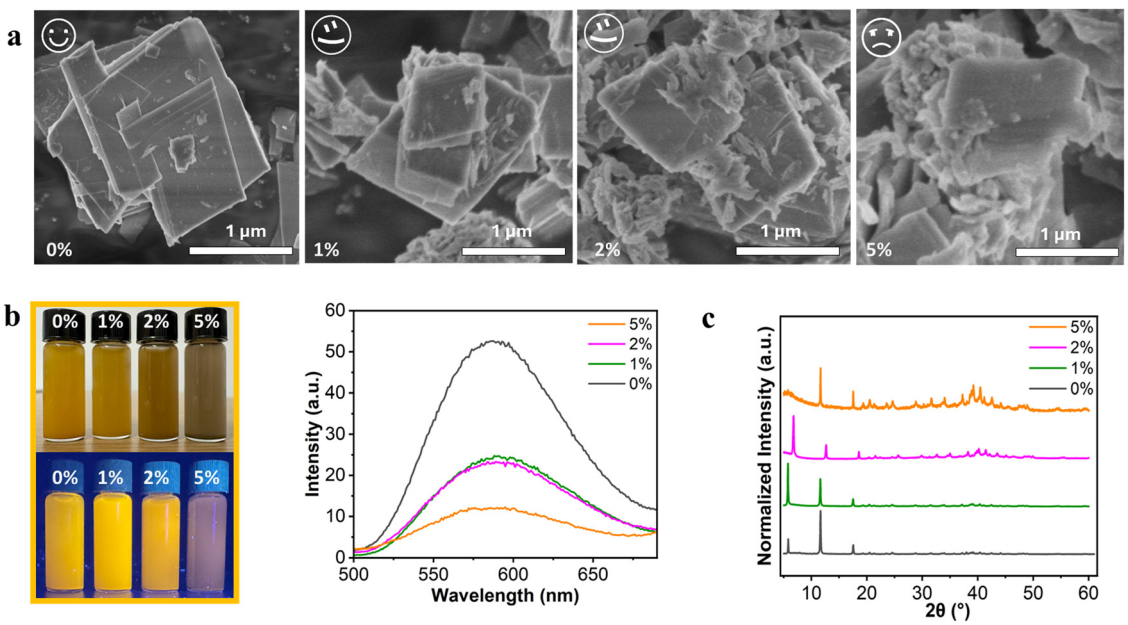

Fig. 5 (a) SEM showing crystal morphology of AgTePh at different tellurium percentages. (b) Images of 0%, 1%, 2% and 5% products in visible light and 365 nm UV lamp. Emission spectra detail the decrease in emission intensity as tellurium percentage increases, consistent with a reduced yield and poorer crystals. (c) Experimental powder pattern of 0%, 1%, 2% & 5%.

poor crystals. Fig. 5c collects X-ray diffraction traces for each of these reaction samples. In the pristine formulation, the low-angle peaks are dominant due to preferred orientation of the product, consistent with a material that is mostly regular crystals that tend to lay flat. In the contaminated samples the high angle peaks are less suppressed by preferred orientation, consistent with the change in crystal morphology. Nevertheless, the products match the pristine phase, so we identified no new phases.

Our experiment demonstrated that a threshold for reaction performance is $<1\%$ tellurium by mass. Tellurium impurity above this threshold substantially impacts the quality of the product, reducing desired optical performance and producing inconsistent crystal morphology. Samples drawn from each contamination rate show a general trend of decreasing performance. The suspension of crystals at 1 mg ml^{-1} is shown in visible light that concludes that the color appears darker at 2% and 5%; the 5% suspended solutions under UV lamp show low luminescence as compared to others.

Conclusion

We have introduced the orange-emitting 2D silver 4-methoxybenzenetellurolate and the 1D red-emitting silver 3-methoxybenzenetellurolate. These compounds were prepared from silver metal and the bis(4-methoxyphenyl) ditelluride and bis(3-methoxyphenyl) ditelluride, respectively synthesized using a Grignard reaction. We found that elemental tellurium byproducts cooccur with the product, and using the crude has a negative impact on the product quality of the resulting MOChas. Specifically, it leads to the formation of smaller crystals with deformed edges and diminished optical qualities. The introduction of methoxy groups at the *meta* and *para* positions led to distinct features such as luminescence, stability, and topology. We find that similar structural properties result in similar emissive properties. AgTe-4M and AgTePh exhibit remarkably similar emissive properties, owing to their structural resemblance. Utilizing a Grignard reaction for the creation of organic precursors allows for the exploration of silver phenyltellurolates and has stimulated further research into their potential optoelectronic uses.

Experimental

Synthesis of silverbenzenetellurolate, AgTePh (tethrene)

For tethrene synthesis, organic precursor diphenyl ditelluride was prepared by Grignard synthesis. A three-necked round bottom flask (100 mL) equipped with a magnetic stir bar was charged with tellurium powder (0.638 g, 5 mmol, 1.0 equiv.). One end of the flask was connected to a Schlenk line, the other end sealed with a septum, while the middle neck was equipped with a reflux condenser. The flask was purged and filled with nitrogen, then 40 mL of dry THF was added through the septum end. The Grignard reagent, phenylmagnesium bromide (5 mmol, 1.0 equiv., 1.0 M solution in THF) was added through the septum end into the suspension of tellurium powder under nitrogen pressure while stirring. The mixture was stirred and refluxed for 4 hours and then poured into 100 mL saturated ammonium chloride solution, bubbled with air for 12 hours, and filtrated. The crude material was purified by column chromatography on silica gel to afford the product. This diphenyl ditelluride was taken in a 1D vial with silver powder and 1 ml methanol and kept in the bead bath at 80 °C for 24 hours. Upon noting the change in color from brown to yellow, the vial was removed and proceeded with the purification process. The recovered product was carefully examined, and it was noted that the quality was not satisfactory. After conducting a comprehensive review, it was discovered that the presence of tellurium in the organic precursor was responsible for this negative effect. The purity of the precursor was improved *via* chromatographic separation using silica gel columns and diethyl ether as mobile phase. Thus, tellurium metal was isolated from the organic precursor diphenyl ditelluride. To test the threshold of this negative effect, tethrene was prepared as per the explained synthetic procedure with the added tellurium 0.01 mg, 0.02 mg, 0.05 mg per mg of the organic precursors to form 1%, 2% and 5% respectively. No tellurium was added to form 0% sample.

Synthesis of silver 3-, and 4-methoxybenzenetellurolate (AgTe-3M & AgTe-4M)

For synthesizing 3-, and 4-methoxybenzenetellurolate, organic precursors bis(4-methoxyphenyl) ditelluride and bis(3-methoxyphenyl) ditelluride were prepared by Grignard synthesis mentioned above, using the Grignard reagents 4-methoxy phenylmagnesium bromide (5 mmol, 1.0 equiv., 1.0 M in THF) and 3-methoxy phenylmagnesium bromide (5 mmol, 1.0 equiv., 1.0 M in THF) respectively.

Synthesis of AgTe-4M

Silver powder, 2–3.5 μm, ≥99.9% trace metals basis obtained from Sigma Aldrich was used to prepare AgTe-4M; silver metal powder and prepared precursor was taken in (1 : 1) molar ratio and added to a 1-dram vial and mixed thoroughly using spatula. 1 mL methanol solvent was added to the vial and mixed. The vial was heated in a metal bead bath (Armor-Beads^{tm}) under the hood at 80 °C for 24 hours. A bright yellow to orange product was observed after 7–8 hours, and reaction was allowed to continue to incubate until stoichiometric conversion. The crystalline product is brightly colored and does not appear mixed with any residual byproducts. Yellow colored crystals appeared indicating the completion of reaction. The vial was removed from the furnace and cooled down for 5–10 minutes, followed by purification.

For purification and isolation, the sample obtained was sonicated for 2 minutes to separate the microcrystals and dismount the product from the walls of the vial. The product was transferred to a 15 ml centrifuge tube with 6–7 mL methanol and centrifuged at 5000 rpm for 10 minutes, followed by decanting the solvent to remove the unreacted ligand. The process was repeated three times, and then crystals were

transferred to watch glass and allowed to air dry for 24 hours. The crystals were transferred in a 0.5-dram vial, dry, and stored in the refrigerator for future use.

Synthesis of AgTe-3M

To prepare AgTe-3M, the same procedure as above was used. The reaction took 4 days for completion.

For purification and isolation, the sample obtained was sonicated for 15 minutes as the crystals were clumped together. The product was transferred to a beaker and gravitational separation by decanting was done to remove the heavier silver impurity. The obtained product was centrifuged and filtered as the previous example.

Author contributions

The manuscript was written through contributions of all authors. All authors have given approval to the final version of the manuscript.

Conflicts of interest

There are no conflicts to declare.

Data availability

Code for generating powder patterns and interfacing with GSAS-II was implemented in a DIALS/CCTBX environment, currently available from https://github.com/cctbx/cctbx-project.

All other data to support the findings of this study have been included in the article and supporting information (SI). Supplementary information: experimental and characterization, thermogravimetric analysis (TGA) data, scanning electron microscopy (SEM) data for AgTe-4M thickness, nuclear magnetic resonance (NMR) data, optical band-gap plot, excitation spectra, comparison with thiolate analogs, energy dispersive X-ray (EDX) data. See DOI: https://doi.org/10.1039/d5ma01354b.

CCDC 2463202 contains the supplementary crystallographic data for this paper.[63]

Acknowledgements

The authors gratefully acknowledge the support and assistance from the user support staff at Diamond Light Source (DLS), United Kingdom for their assistance in collecting crystallography data (Proposal cy35300-1). SEM work was performed at the Biosciences Electron Microscopy Facility of the University of Connecticut on the FEI NovaSEM 450 with assistance and training from Dr Xuanhao Sun. The authors express gratitude for the preliminary characterization analytical assistance provided by Dr Morales and Dr Ndaya at University of Connecticut. The authors would also like to thank and acknowledge the support from the US Department of Energy Integrated Computational and Data Infrastructure for Scientific Discovery grant DE-SC0022215. M.C.W. gratefully acknowledges the National Science Foundation Graduate Research Fellowship under Grant No. DGE 2136520.

References

1 K. Yao, M. S. Collins, K. M. Nell, E. S. Barnard, N. J. Borys, T. Kuykendall, J. N. Hohman and P. J. Schuck, *ACS Nano*, 2021, **15**, 4085–4092.
2 D. C. Popple, E. A. Schriber, M. Yeung and J. N. Hohman, *Langmuir*, 2018, **34**, 14265–14273.
3 B. Trang, M. Yeung, D. C. Popple, E. A. Schriber, M. A. Brady, T. R. Kuykendall and J. N. Hohman, *J. Am. Chem. Soc.*, 2018, **140**, 13892–13903.
4 M. Aleksich, D. W. Paley, E. A. Schriber, W. Linthicum, V. Oklejas, D. W. Mittan-Moreau, R. P. Kelly, P. A. Kotei, A. Ghodsi, R. G. Sierra, A. Aquila, F. Poitevin, J. P. Blaschke, M. Vakili, C. J. Milne, F. Dall'Antonia, D. Khakhulin, F. Ardana-Lamas, F. Lima, J. Valerio, H. Han, T. Gallo, H. Yousef, O. Turkot, I. J. Bermudez Macias, T. Kluyver, P. Schmidt, L. Gelisio, A. R. Round, Y. Jiang, D. Vinci, Y. Uemura, M. Kloos, M. Hunter, A. P. Mancuso, B. D. Huey, L. R. Parent, N. K. Sauter, A. S. Brewster and J. N. Hohman, *J. Am. Chem. Soc.*, 2023, **145**, 17042–17055.
5 T. Sakurada, Y. Cho, W. Paritmongkol, W. S. Lee, R. Wan, A. Su, W. Shcherbakov-Wu, P. Müller, H. J. Kulik and W. A. Tisdale, *J. Am. Chem. Soc.*, 2023, **145**, 5183–5190.
6 E. A. Schriber, D. W. Paley, R. Bolotovsky, D. J. Rosenberg, R. G. Sierra, A. Aquila, D. Mendez, F. Poitevin, J. P. Blaschke, A. Bhowmick, R. P. Kelly, M. Hunter, B. Hayes, D. C. Popple, M. Yeung, C. Pareja-Rivera, S. Lisova, K. Tono, M. Sugahara, S. Owada, T. Kuykendall, K. Yao, P. J. Schuck, D. Solis-Ibarra, N. K. Sauter, A. S. Brewster and J. N. Hohman, *Nature*, 2022, **601**, 360–365.
7 C. Kastl, P. Bonfà and L. Maserati, *Adv. Opt. Mater.*, 2023, **11**(7), 2202213.
8 L. Maserati, S. Refaely-Abramson, C. Kastl, C. T. Chen, N. J. Borys, C. N. Eisler, M. S. Collins, T. E. Smidt, E. S. Barnard, M. Strasbourg, E. A. Schriber, B. Shevitski, K. Yao, J. N. Hohman, P. J. Schuck, S. Aloni, J. B. Neaton and A. M. Schwartzberg, *Mater. Horiz.*, 2021, **8**, 197–208.
9 T. Sakurada, N. Pathoor, T. Matsumoto, R. Khamlue, P. Chatsiri, J. Valenta, T. Kawamoto, S. Omagari, W. A. Tisdale, W. Paritmongkol, Y. Cho and M. Vacha, *J. Am. Chem. Soc.*, 2024, **36**(10), 5238–5249.
10 X. Yun, J. Nie, H. Hu, H. Zhong, D. Xu, Y. Shi and H. Li, *Nanomaterials*, 2024, **14**(1), 46.
11 M. Adnan, J. J. Baumberg and G. Vijaya Prakash, *Sci. Rep.*, 2020, **10**, 2615.
12 X. Huang and J. Li, *J. Am. Chem. Soc.*, 2007, **129**, 3157–3162.
13 E. A. Schriber, D. C. Popple, M. Yeung, M. A. Brady, S. A. Corlett and J. N. Hohman, *ACS Appl. Nano Mater.*, 2018, **1**, 3498–3508.
14 C. Lavenn, L. Okhrimenko, N. Guillou, M. Monge, G. Ledoux, C. Dujardin, R. Chiriac, A. Fateeva and A. Demessence, *J. Mater. Chem. C Mater.*, 2015, **3**, 4115–4125.

15 O. Veselska, D. Podbevšek, G. Ledoux, A. Fateeva and A. Demessence, *Chem. Commun.*, 2017, **53**, 12225–12228.
16 I. G. Dance, K. J. Fisher and R. M. Herath Banda, *Inorg. Chem.*, 1991, **30**(2), 183–187.
17 C. Lavenn, N. Guillou, M. Monge, D. Podbevšek, G. Ledoux, A. Fateeva and A. Demessence, *Chem. Commun.*, 2016, **52**, 9063–9066.
18 X. Huang, H. R. Heulings IV, V. Le and J. Li, *Chem. Mater.*, 2001, **13**, 3754–3759.
19 H. Yan, J. N. Hohman, F. H. Li, C. Jia, D. Solis-Ibarra, B. Wu, J. E. P. Dahl, R. M. K. Carlson, B. A. Tkachenko, A. A. Fokin, P. R. Schreiner, A. Vailionis, T. R. Kim, T. P. Devereaux, Z. X. Shen and N. A. Melosh, *Nat. Mater.*, 2017, **16**, 349–355.
20 B. Choi, K. Jo, M. Rahaman, A. Alfieri, J. Lynch, G. K. Pribil, H. Koh, E. A. Stach and D. Jariwala, *ACS Nano*, 2024, **18**, 25489–25498.
21 H. A. Mills, C. G. Jones, K. P. Anderson, A. D. Ready, P. I. Djurovich, S. I. Khan, J. N. Hohman, H. M. Nelson and A. M. Spokoyny, *Chem. Mater.*, 2022, **34**, 6933–6943.
22 P. A. Kotei, D. W. Paley, V. Oklejas, D. W. Mittan-Moreau, E. A. Schriber, M. Aleksich, M. C. Willson, I. Inoue, S. Owada, K. Tono, M. Sugahara, S. Inaba-Inoue, A. Aquila, F. Poitevin, J. P. Blaschke, S. Lisova, M. S. Hunter, R. G. Sierra, J. A. Gascón, N. K. Sauter, A. S. Brewster and J. N. Hohman, *Small Sci.*, 2024, **4**(1), 2470002.
23 M. Aleksich, Y. Cho, D. W. Paley, M. C. Willson, H. N. Nyiera, P. A. Kotei, V. Oklejas, D. W. Mittan-Moreau, E. A. Schriber, K. Christensen, I. Inoue, S. Owada, K. Tono, M. Sugahara, S. Inaba-Inoue, M. Vakili, C. J. Milne, F. DallAntonia, D. Khakhulin, F. Ardana-Lamas, F. Lima, J. Valerio, H. Han, T. Gallo, H. Yousef, O. Turkot, I. J. B. Macias, T. Kluyver, P. Schmidt, L. Gelisio, A. R. Round, Y. Jiang, D. Vinci, Y. Uemura, M. Kloos, A. P. Mancuso, M. Warren, N. K. Sauter, J. Zhao, T. Smidt, H. J. Kulik, S. Sharifzadeh, A. S. Brewster and J. N. Hohman, *Adv. Funct. Mater.*, 2025, **35**(6), 2414914.
24 R. Khamlue, P. Chatsiri, T. Sakurada, J. Chotimook, P. Leangtanom, P. Prayongkul, T. Atithep, J. Padchasri, P. Kidkhunthod, M. Vacha, P. Pattanasattayavong and W. Paritmongkol, *J. Am. Chem. Soc.*, 2025, **147**(41), 37242–37254.
25 K.-F. Li, C.-H. Yu, G.-L. Liang, J. Chen, Y. Chang, G. Xu and G.-E. Wang, *Nat. Commun.*, 2025, **16**, 1560.
26 Y. Wen, G.-E. Wang, X. Jiang, X. Ye, W. Li and G. Xu, *Angew. Chem., Int. Ed.*, 2021, **60**, 19710–19714.
27 M. Yeung, D. C. Popple, E. A. Schriber, S. J. Teat, C. M. Beavers, A. Demessence, T. R. Kuykendall and J. N. Hohman, *ACS Appl. Nano Mater.*, 2020, **3**, 3568–3577.
28 H. Rabl, S. N. Myakala, J. Rath, B. Fickl, J. S. Schubert, D. H. Apaydin and D. Eder, *Commun. Chem.*, 2023, **6**, 43.
29 S. Nagaraju Myakala, H. Rabl, J. S. Schubert, S. Batool, P. Ayala, D. H. Apaydin, A. Cherevan and D. Eder, *Small*, 2024, **20**(33), 2400348.
30 W. S. Lee, Y. Cho, E. R. Powers, W. Paritmongkol, T. Sakurada, H. J. Kulik and W. A. Tisdale, *ACS Nano*, 2022, **16**, 20318–20328.
31 W. Paritmongkol, Z. Feng, S. Refaely-Abramson, W. A. Tisdale, C. Kastl and L. Maserati, *ACS Nano*, 2025, **19**(13), 12467–12477.
32 L. T. Nguyen, R. A. Zupnick, Q. Vo Truong and T. L. Atallah, *Nanoscale*, 2025, **17**, 19136–19142.
33 G.-E. Wang, S. Luo, T. Di, Z. Fu and G. Xu, *Angew. Chem., Int. Ed.*, 2022, **61**, e202203151.
34 A. C. Hernandez Oendra, M. A. Aspect, J. L. Jaeggi, J. Baumann, C. R. Lightner, A. B. Pun and D. J. Norris, *Chem. Mater.*, 2023, **35**, 9390–9398.
35 W. S. Lee, P. Müller, N. Samulewicz, T. Deshpande, R. Wan and W. A. Tisdale, *Chem. Mater.*, 2024, **36**, 9904–9913.
36 Q. Fan, M. C. Willson, K. A. Foell, D. W. Paley, P. A. Kotei, E. A. Schriber, D. J. Rosenberg, K. Rani, D. M. Tchoń, M. Zeller, C. Melendrez, J. Kang, I. Inoue, S. Owada, K. Tono, M. Sugahara, A. S. Brewster and J. N. Hohman, *J. Am. Chem. Soc.*, 2024, **146**(44), 30349–30360.
37 E. A. Schriber, D. J. Rosenberg, R. P. Kelly, A. Ghodsi and J. N. Hohman, *Front. Chem.*, 2021, **9**, 593637.
38 W. Paritmongkol, T. Sakurada, W. S. Lee, R. Wan, P. Müller and W. A. Tisdale, *J. Am. Chem. Soc.*, 2021, **143**, 20256–20263.
39 W. Paritmongkol, W. S. Lee, W. Shcherbakov-Wu, S. K. Ha, T. Sakurada, S. J. Oh and W. A. Tisdale, *ACS Nano*, 2022, **16**, 2054–2065.
40 I. D. Sadekov and A. V. Zakharov, *Russ. Chem. Rev.*, 1999, **68**, 909–923.
41 C. W. Sink and A. B. Harvey, *J. Chem. Phys.*, 1972, **57**, 4434–4442.
42 K. Hamada and H. Morishita, *Synth. React. Inorg. Met.-Org. Chem.*, 1977, **7**, 355–366.
43 B. Khater, J. C. Guillemin, G. Bajor and T. Veszprémi, *Inorg. Chem.*, 2008, **47**, 1502–1511.
44 D. R. Allan, H. Nowell, S. A. Barnett, M. R. Warren, A. Wilcox, J. Christensen, L. K. Saunders, A. Peach, M. T. Hooper and L. Zaja, *Crystals*, 2017, **7**, 336.
45 E. A. Weiss, *ACS Nano*, 2021, **15**(3), 3568–3577.
46 O. Veselska, N. Guillou, G. Ledoux, C. C. Huang, K. D. Newell, E. Elkaïm, A. Fateeva and A. Demessence, *Nanomaterials*, 2019, **9**, 1408.
47 X. Zhou, X. Hu, J. Yu, S. Liu, Z. Shu, Q. Zhang, H. Li, Y. Ma, H. Xu and T. Zhai, *Adv. Funct. Mater.*, 2018, **28**, 1706587.
48 S. C. Smith, W. Bryks and A. R. Tao, *Langmuir*, 2019, **35**, 2887–2897.
49 R. Khamlue, T. Sakurada, Y. Cho, W. S. Lee, P. Leangtanom, M. G. Taylor, W. Naewthong, P. Sripetch, B. Na Ranong, T. Autila, T. Rungseesumran, J. Kaewkhao, T. Sudyoadsuk, A. Kopwitthaya, P. Müller, V. Promarak, H. J. Kulik, W. A. Tisdale and W. Paritmongkol, *Chem. Mater.*, 2024, **36**, 5238–5249.
50 M. C. Willson, D. W. Paley, E. A. Schriber, D. J. Rosenberg, D. M. Tchoń, P. A. Kotei, K. Rani, C. Melendrez, M. Zeller, T. Kaushik, Q. Fan, C. Dehiwala Liyanage, J. Kang, I. Inoue, K. Tono, Y. Inubushi, A. S. Brewster and J. N. Hohman, *Inorg. Chem.*, 2025, **64**, 16877–16888.
51 J. Jellinek, U. Salian and S. Srinivas, Scientific and technical aerospace reports.

52 H. Schmidbaur and A. Schier, *Angew. Chem., Int. Ed.*, 2015, **54**, 746–784.
53 S. Kintzel, K. Eckhardt, J. Getzschmann, V. Bon, J. Grothe and S. Kaskel, *Eur. J. Inorg. Chem.*, 2020, 3167–3173.
54 A. Kovalevskiy, C. Yin, J. Nuss, U. Wedig and M. Jansen, *Chem. Sci.*, 2019, **11**, 962.
55 M. Palusiak and S. J. Grabowski, *J. Mol. Struct.*, 2002, **642**, 97–104.
56 C. Shivanna, S. M. Patil, C. Mallikarjunaswamy, R. Ramu, P. Akhileshwari, L. R. Nagaraju, M. A. Sridhar, S. A. Khanum, V. L. Ranganatha, E. Silina, V. Stupin and R. R. Achar, *Crystals*, 2022, **12**, 960.
57 G. R. Desiraju, The C–H···O Hydrogen Bond: Structural Implications and Supramolecular Design, *Acc. Chem. Res.*, 1996, **29**(9), 441–449.
58 G. Desiraju and T. Steiner, *The Weak Hydrogen Bond*, Oxford University Press, 2010.
59 X. Huang, J. Li and H. Fu, *J. Am. Chem. Soc.*, 2000, DOI: 10.1021/ja002224n.
60 Z. Ajoyan, G. A. Mandl, P. R. Donnarumma, V. Quezada-Novoa, H. A. Bicalho, H. M. Titi, J. A. Capobianco and A. J. Howarth, *ACS Mater. Lett.*, 2022, **4**, 1025–1031.
61 S. Hawila, F. Massuyeau, R. Gautier, A. Fateeva, S. Lebègue, W. J. Kim, G. Ledoux, A. Mesbah and A. Demessence, *J. Mater. Chem. B*, 2023, **11**, 3979–3984.
62 S. Trabelsie, A. Samet, H. Dammak, F. Michaud, L. Santos, Y. Abid and S. Chaabouni, *Opt. Mater.*, 2019, **89**, 355–360.
63 CCDC 2463202: Experimental Crystal Structure Determination, 2026, DOI: 10.5517/ccdc.csd.cc2np54p.